Science Advances

AAAS

advances.sciencemag.org/cgi/content/full/4/6/eaaq1702/DC1

Supplementary Materials for

The neuronal S100B protein is a calcium-tuned suppressor of amyloid-β aggregation

Joana S. Cristóvão, Vanessa K. Morris, Isabel Cardoso, Sónia S. Leal, Javier Martínez, Hugo M. Botelho, Christoph Göbl, Rodrigo David, Katrin Kierdorf, Mobina Alemi, Tobias Madl, Günter Fritz, Bernd Reif, Cláudio M. Gomes

Published 29 June 2018, *Sci. Adv.* **4**, eaaq1702 (2018)
DOI: 10.1126/sciadv.aaq1702

This PDF file includes:

Supplementary Methods

Aβ25-35 aggregation assays

Synthetic Aβ25-35 (Bachem) was pre-treated overnight with 1,1,1,3,3,3-Hexafluoro-2-propanol (HFIP) and lyophilized. Prior to the aggregation assay Aβ25-35 stock was redissolved in CH_3CN/H_2O 65:35 (v/v) and two-fold diluted in 50mM phosphate buffer pH7.4 to a final concentration of 500 μM. ThT fluorescence intensity was monitored at 480nm upon excitation at 440 nm using 50 μM of Aβ25-35 in 50 mM phosphate buffer, 0.1 mM EDTA and 10 μM of ThT, at increasing concentrations of S100B (50-200 μM) at 37°C under quiescent conditions.

Dot Blotting using anti-amyloid antibodies

Aβ42 aggregates obtained at the plateau phase of each aggregation kinetic curve were diluted four times and dotted in triplicates onto a PVDF membrane and probed with a 1000x dilution of the anti-amyloid fibril OC (AB9234, Merck Millipore) and A11 (AB9234, Merck Millipore) antibodies according to manufacturer's instructions.

Analysis of S100B expression in Alzheimer's Disease animal model

For analysis of S100B in a transgenic Alzheimer animal model, 16-weeks-old male B6.Cg-Tg(APPSwFlLon,PSEN1*M146L*L286V)6799Vas/Mmjax (5XFAD) mice were used. These mice overexpress the K670N/M671L (Swedish), I716V (Florida), and V717I (London) mutations in human APP (695), as well as M146L and L286V mutations in human PS1. Age-matched male littermate control animals served as a control. After anaesthetization, mice were transcardially perfused with PBS and subsequently with 4% paraformaldehyde and brains were embedded in paraffin. Sagittal sections of 3 μm were obtained from the brains and stained by immunohistochemistry as described previously with minor modifications. S100B was detected with an anti-S100B antibody (DAKO Ltd.); the antibody was added overnight at a dilution of 1:1000. Staining was performed with Anti-Rabbit-HRP and chromogenic substrate DAB and counterstained with hematoxylin. Stained sections were analysed using a conventional microscope (Olympus BX-61) equipped with a colour camera (Olympus DP71). Staining of S100B was quantified with ImageJ.

Supplementary figures

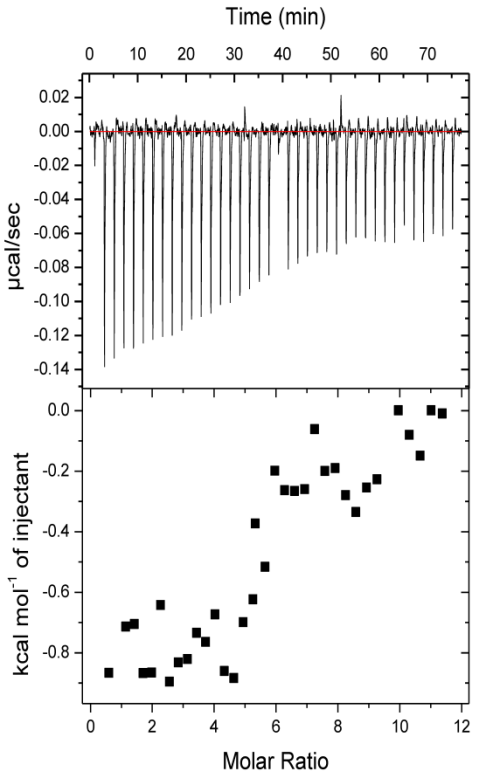

fig. S1. Isothermal titration calorimetry analysis of the Aβ42/S100B interaction. The upper panel shows raw heat of binding and the lower panel the integrated data obtained after subtracting the heat of dilution from the buffer.

$$A\beta42 + S100B \underset{}{\overset{k_{obs}}{\leftrightarrows}} A\beta42{:}S100B$$

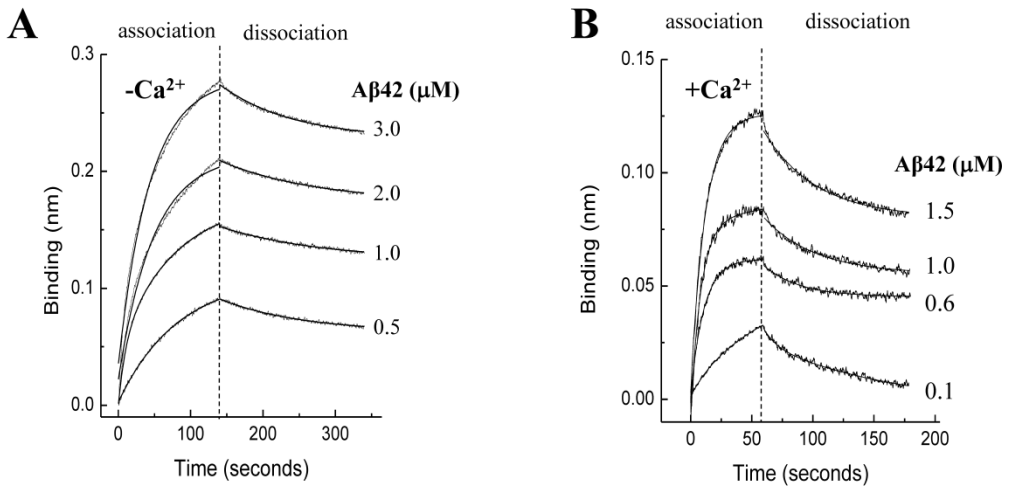

Aβ42:S100B

Aβ (μM)	k_{obs} (s^{-1})	k_d (s^{-1})	k_a ($\mu M^{-1}.s^{-1}$)	K_D * (μM)
0.5	1.22E-02	8.77E-03	6.86E-03	1.28
1.0	2.26E-02	7.04E-03	1.56E-02	0.45
2.0	2.08E-02	7.58E-03	6.61E-03	1.2
3.0	2.36E-02	1.01E-02	4.5E-03	2.2
Average		8.4E-03		1.3

Aβ42:Ca^{2+}-S100B

Aβ (μM)	k_{obs} (s^{-1})	k_d (s^{-1})	k_a ($\mu M^{-1}.s^{-1}$)	K_D * (μM)
0.1	2.15E-02	1.81E-02	3.50E-02	0.51
0.6	9.35E-02	3.45E-02	9.80E-02	0.35
1.0	1.11E-01	2.38E-02	8.72E-02	0.27
1.5	8.40E-02	2.32E-02	4.05E-02	0.57
Average		2.49E-02		0.43

fig. S2. BLI analysis of the Aβ42/S100B interaction. Aligned sensorgram traces showing Aβ42 association and dissociation steps to immobilized S100B at pH 7.4 by Bio-layer interferometry. The obtained sensorgrams evidence an increase in the saturation response with increasing Aβ42 concentrations in the absence (**A**) and in the presence (**B**) of 5mM $CaCl_2$. The corresponding interaction kinetic parameters are presented in tables below the sensorgrams. The determined dissociation constants (K_D) for the complex average to 1.3 and 0.43 μM in the absence and in the presence of $CaCl_2$.

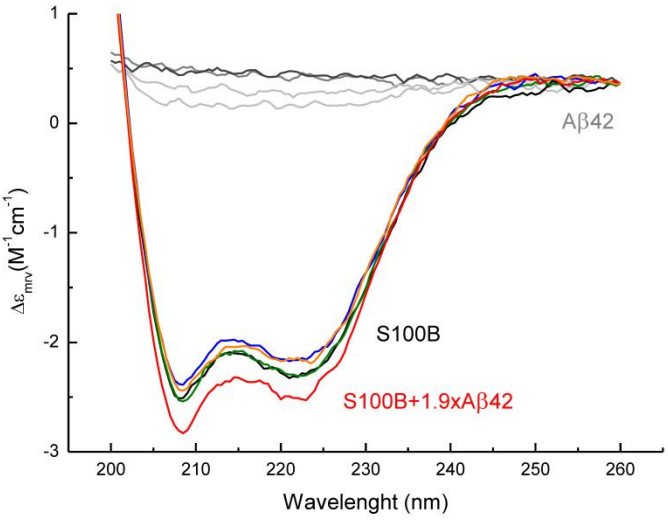

fig. S3. CD analysis of the Aβ42/S100B interaction in the absence of $CaCl_2$. Far UV-CD spectra of 4μM apo-S100B (Black) and after overnight incubation at 4ºC, in the presence of Aβ42 at increasing S100B:Aβ42 ratios: 0.25 (green), 0.5 (blue), 1 (orange) and 1.9 (red).

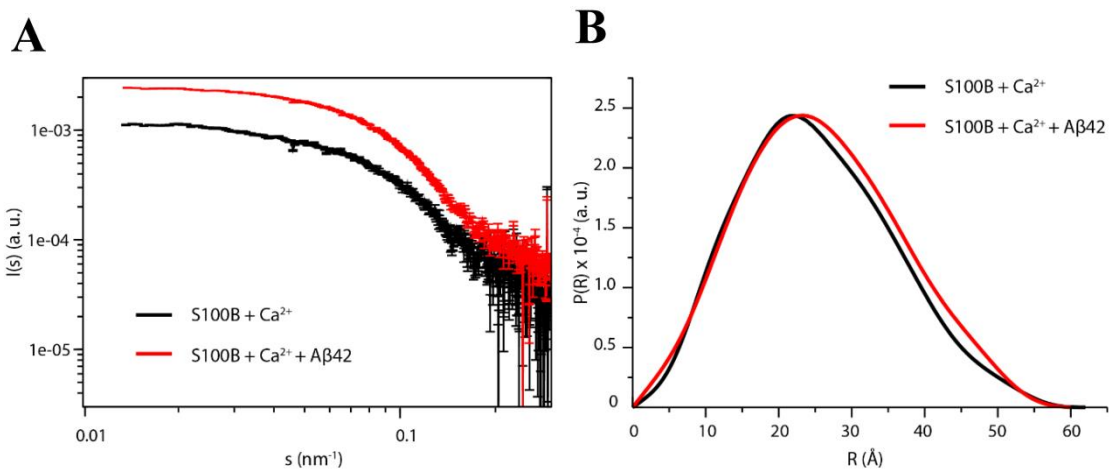

fig. S4. SAXS analysis of the Aβ42/S100B complex. (**A**) Raw SAXS scattering data of S100B and S100B with Aβ42 in a 1:1 molar ratio, both in the presence of calcium. (A) Comparison of the pair distance distribution functions.

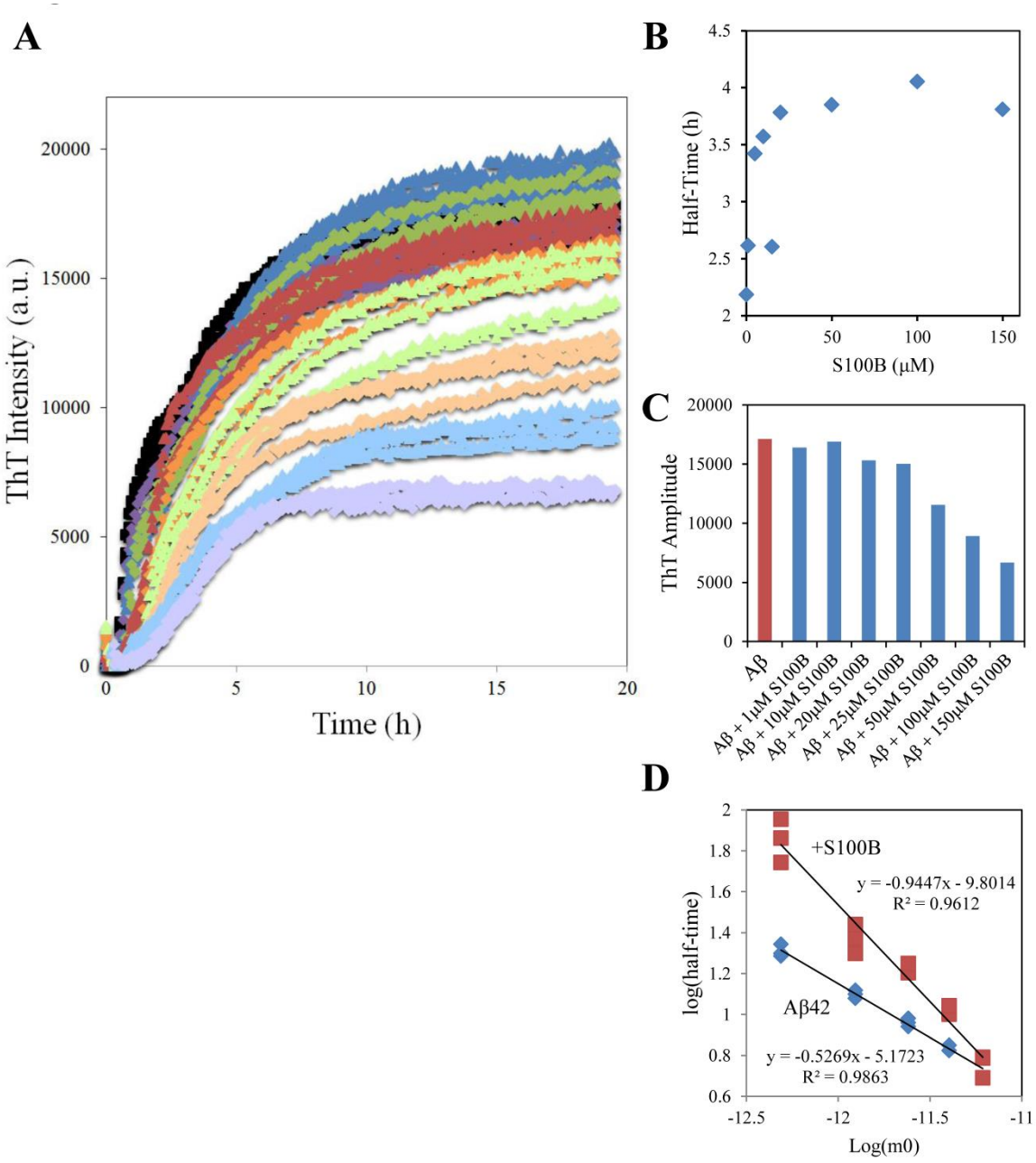

fig. S5. Effect of apo-S100B over Aβ42 aggregation in a fragmentation-dominated regime. For these experiments Aβ42 aggregation proceeded in 50 mM HEPES pH 7.4, 0.5 mM EDTA, 5 mM TCEP at 37ºC, with 20s agitation at 86 rpm every 400s. (**A**) Aggregation of 5 μM Aβ42 (Black) proceeded at increasing concentrations of apo-S100B: 1μM (purple), 5μM (dark blue), 10 μM (dark green), 15 μM (red), 20 μM (orange), 25 μM (Light green), 50 μM (light orange), 100 μM (light blue) and 150 μM (light purple). Plots represent averaged curves obtained from 3 independent replicates (n=3) for each of the tested conditions. (**B**) Plot of the Aβ42 aggregation half-times in the presence of 0.5 mM EDTA as a function of S100B. (**C**) Plot of the ThT intensity at the end-points of the aggregation of 5 μM Aβ42 in the presence of 0.5 mM EDTA at increasing concentrations of apo-S100B. (**D**) Log-Log plot of the half-time of the Aβ42 aggregation reaction as a function of initial Aβ42 monomer concentration in the absence and in the presence of excess S100B (15:1).

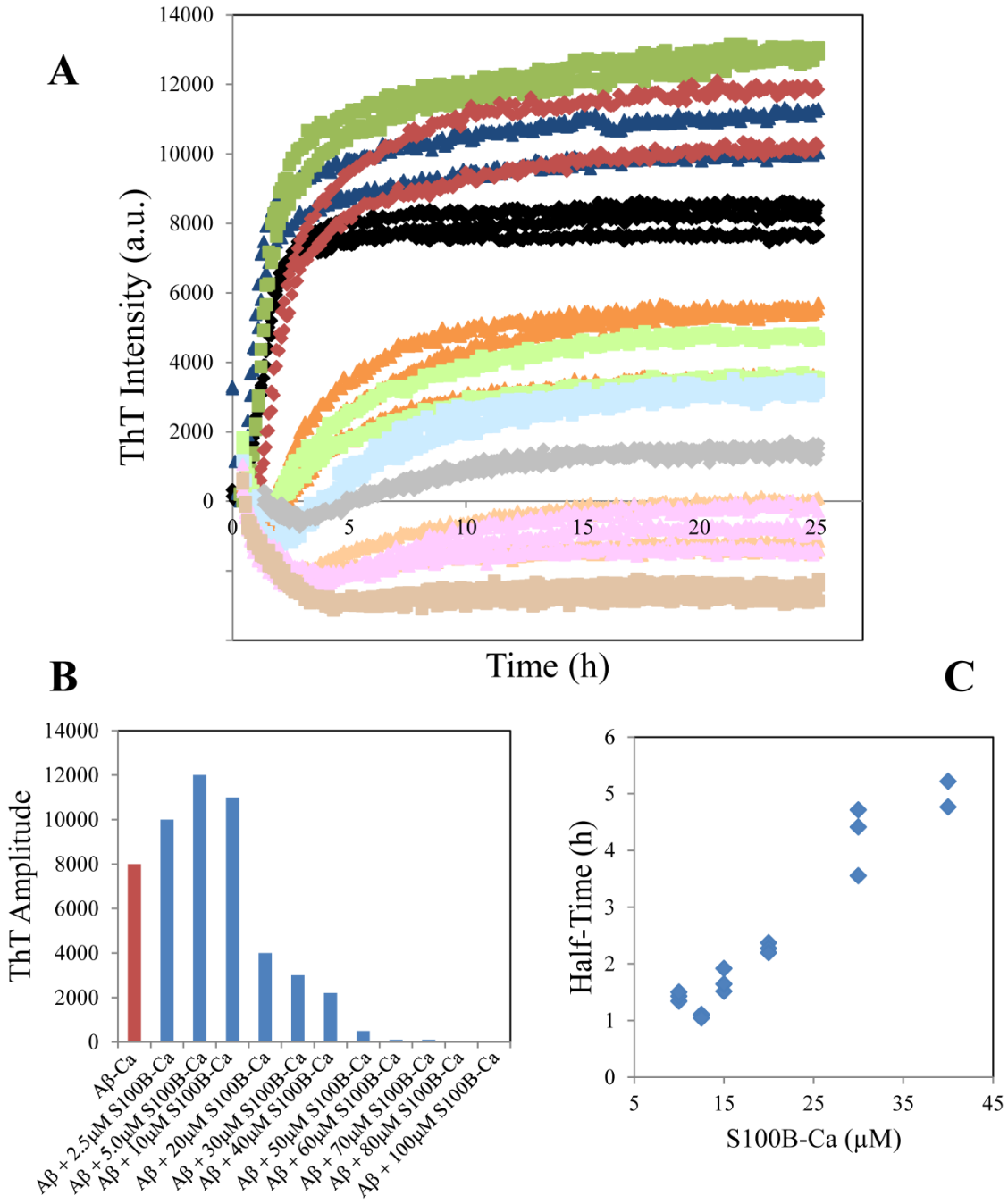

fig. S6. Effect of Ca^{2+}-S100B over Aβ42 aggregation in a fragmentation-dominated regime. For these experiments Aβ42 aggregation proceeded in 50 mM HEPES pH 7.4, 5 mM TCEP and 1.1 mM $CaCl_2$ at 37ºC, with 20s agitation at 86 rpm every 400s. (**A**) Aggregation of 10 μM Aβ42 (Black) proceeded at increasing concentrations of apo-S100B: 2.5 μM (dark blue), 5 μM (dark green), 10 μM (red), 20 μM (orange), 30 μM (Light green), 40 μM (light blue), 50μM (gray); 60μM (light orange), 70 μM (light pink) and 80 μM (brown). Plots represent averaged curves obtained from 3 independent replicates (n=3) for each of the tested conditions. (**B**) Plot of the ThT intensity at the end-points of the aggregation of 10 μM Aβ42 in the in the presence of calcium at increasing concentrations of Ca^{2+}-S100B. (**C**) Plot of the Aβ42 aggregation half-times in the presence of calcium as a function of Ca^{2+}-S100B. Triangles represent averaged values obtained from 3 independent replicates (n=3) for each of the tested conditions.

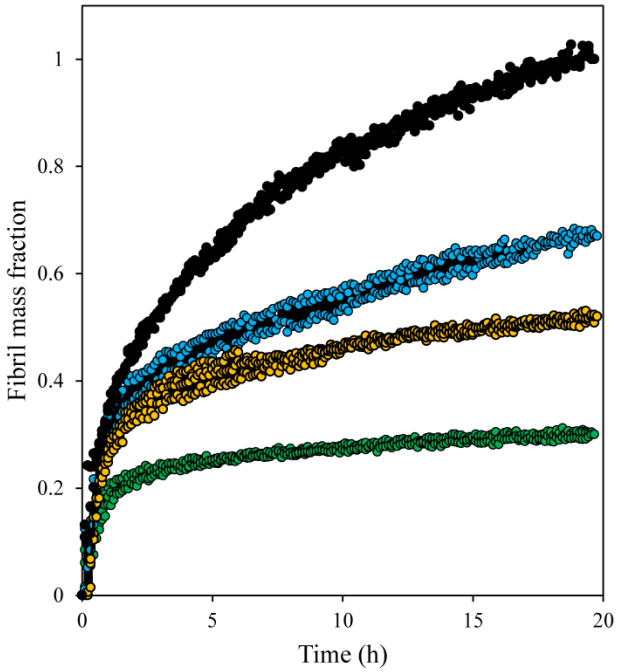

fig. S7. S100B inhibits Aβ25–35 aggregation. Aggregation of 25 μM Aβ25-35 proceeded in 50 mM HEPES pH 7.4 at 37ºC under quiescent conditions in the presence of increasing S100B: 25 μM (blue), 50 μM (yellow) and 100 μM (green). Plots represent averaged curves obtained from 3 independent replicates (n=3) for each of the tested conditions.

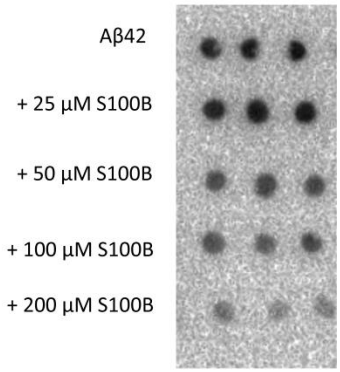

fig. S8. Dot blot analysis of Aβ42 aggregates formed in the presence of S100B. The conformational anti-amyloid fibril antibody (OC) was employed and the experiments were done in triplicate.

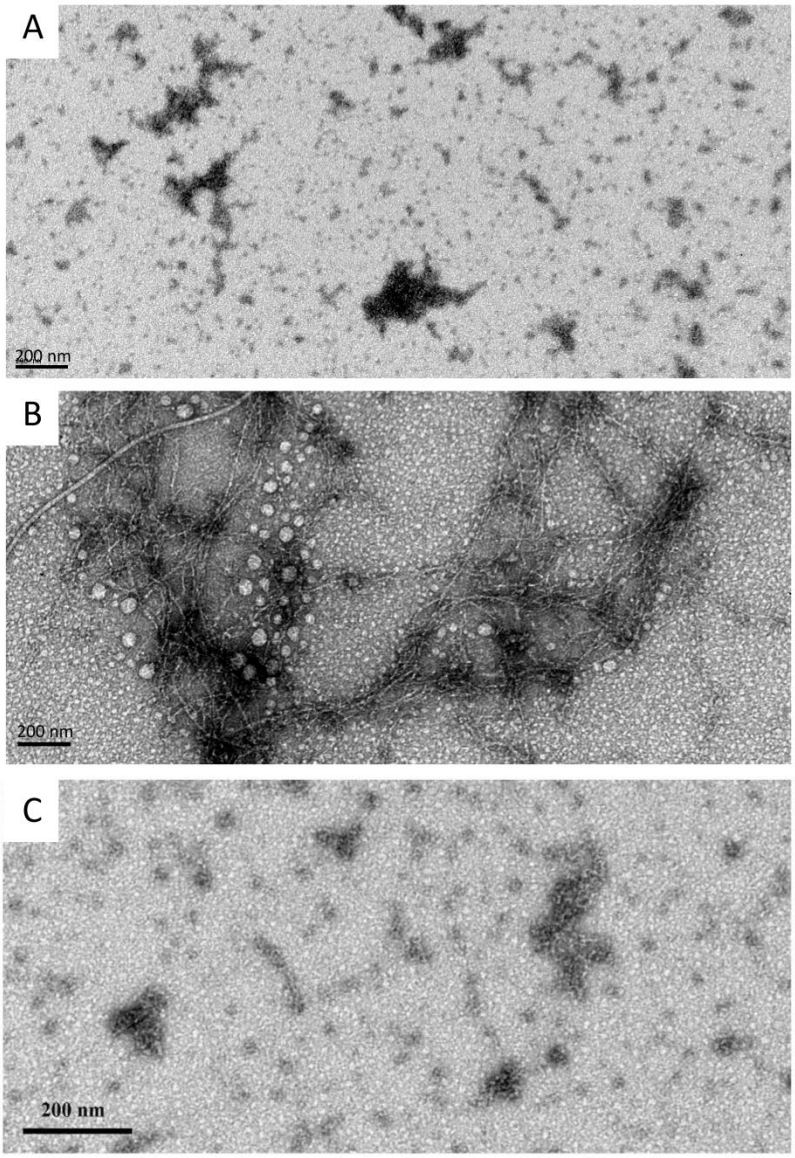

fig. S9. TEM images of Aβ aggregates formed in the presence and absence of S100B. Samples were taken from end-points of the ThT aggregation kinetics plots. (**A**) 150 μM S100B with 1.1 mM $CaCl_2$; (**B**) 10 μM Aβ42 with 1.1 mM $CaCl_2$; and (**C**) 10 μM Aβ42 + 150 μM S100B and 1.1 mM $CaCl_2$.

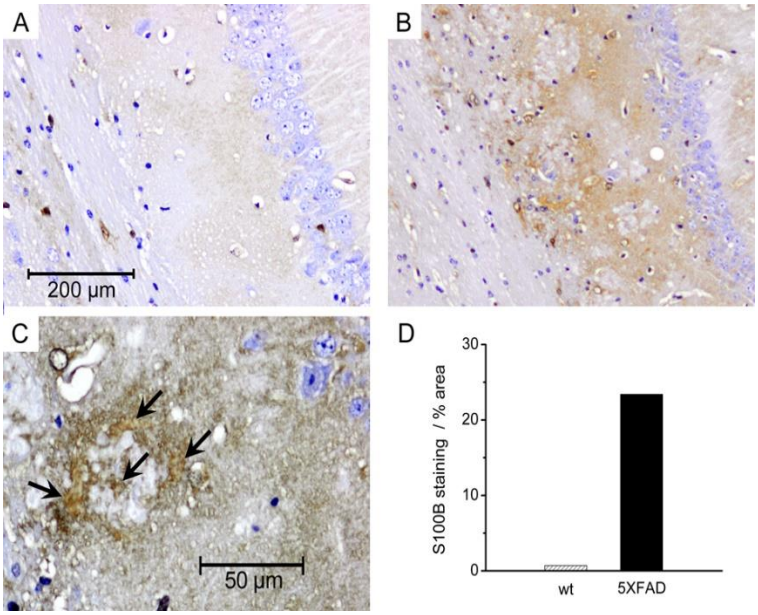

fig. S10. S100B accumulates at high levels around plaques in AD mice brains. Amyloid deposits form mainly in the cortex and hippocampus and the highest amyloid plaques load is observed in subfields of the latter brain area. Therefore we focused the analysis of expression and localization of S100B on the hippocampus. (A,B) The area around the granule cell layer at the dentate gyrus of the hippocampus is shown. In wild-type animals S100B levels are in general low. In several S100B+ cells are observed, which exhibit high levels of intracellular S100B. In contrast, 5XFAD mice show massive staining for S100B right below the granule cell layer (GCL) around amyloid plaques, which appear as bright areas due to their strong refraction of light. The staining for S100B is not limited to cell bodies; rather covers large areas and indicates a diffuse distribution of S100B but also very high levels of the protein around the plaques. This staining pattern clearly shows that S100B is present at high concentrations in the tissue and suggests high levels of extracellular S100B. The most intensive staining for S100B is observed at the plaque border and some intensive patches are detected within the amyloid plaques (C). Quantification of the staining revealed that the area stained for S100B is about 30-fold larger in brain sections of 5XFAD animals compared to age-matched wild type animals (D).